Surface Water and Ocean Topography (SWOT) Project

SWOT Algorithm Theoretical Basis Document
Long Name: Level 1B KaRIn high rate single look complex data science algorithm software
Short Name: L1B_HR_SLC

Initial Release

Document Custodians:

Xiaoqing Wu JPL Algorithm Engineer	Date	Damien Desroches CNES Algorithm Engineer	Date

Approved by:

Curtis Chen JPL Algorithm System Engineer	Date	Roger Roger Fjørtoft CNES Algorithm System Engineer	Date

Concurred by:

Tamlin Pavelsky JPL Hydrology Lead	Date	Jean Francois Cretaux CNES Hydrology Lead	Date

Paper copies of this document may not be current and should not be relied on for official purposes. The current version is in the JPL Product Data Management System (EPDM: https://epdm.jpl.nasa.gov) and the CNES Product Data Management System

See Sect 1.4 for how to cite this document

July 13, 2023
JPL D-105503

National Aeronautics and Space Administration
Jet Propulsion Laboratory
California Institute of Technology

Contributing Authors

Name	Affiliation
Xiaoqing Wu	Jet Propulsion Laboratory

Science Team Reviewers

Name	Affiliation
Scott Hensley	JPL
Herve Yesou	SERTIT

Change Log

VERSION	DATE	SECTIONS CHANGED	REASON FOR CHANGE
Initial Release	2023-07-13	ALL	Initial Release Approved for public release (URS317510/CL#23-3526)

Table of Contents

Contributing Authors **2**

Science Team Reviewers **2**

Change Log **3**

Table of Contents **4**

Table of Figures **6**

Table of Tables **6**

List of TBC Items **7**

List of TBD Items **7**

1 Introduction **8**
1.1 Purpose **8**
1.2 Scope **8**
1.3 Document Organization **8**
1.4 Citing This Document **8**

2 Overview **9**
2.1 Background and Context **9**
2.2 Functional Flow **9**

3 Algorithm Descriptions **12**
3.1 Generate TVP file **12**
3.1.1 Purpose 12
3.1.2 Input Data 12
3.1.3 Output Data 13
3.1.4 Mathematical Statement 13
3.1.5 TVP Parameter Interpolation Accuracy 13
3.2 Extract range reference function **14**
3.2.1 Purpose 14
3.2.2 Input Data 14
3.2.3 Output Data 14
3.2.4 Mathematical Statement 14
3.2.5 Range Reference Function Accuracy 15
3.3 Range Compression **15**
3.3.1 Purpose 15
3.3.2 Input Data 16
3.3.3 Output Data 16
3.3.4 Mathematical Statement 16
3.3.5 Range Compression Accuracy 17
3.4 Doppler Centroid Estimation and Attitude correction **17**
3.4.1 Purpose 17
3.4.2 Input Data 18
3.4.3 Output Data 18
3.4.4 Mathematical Statement 18

3.4.5 Doppler Centroid Accuracy 19
3.5 Generate GrDEM 20
3.5.1 Purpose 20
3.5.2 Input Data 21
3.5.3 Output data 21
3.5.4 Mathematical Statement 21
3.5.5 GrDEM Accuracy 24
3.6 Calculate Image Grids 25
3.6.1 Purpose 25
3.6.2 Input Data 25
3.6.3 Output Data 25
3.6.4 Mathematical Statement 25
3.6.5 Accuracy 26
3.7 Determine sensor illumination position 27
3.7.1 Purpose 27
3.7.2 Input Data 27
3.7.3 Output Data 27
3.7.4 Mathematical Statement 28
3.7.5 Accuracy 29
3.8 Azimuth Compression 29
3.8.1 Purpose 29
3.8.2 Input Data 29
3.8.3 Output Data 29
3.8.4 Mathematical Statement 29
3.8.5 Accuracy 31
3.9 Radiometric Calibration 33
3.9.1 Purpose 33
3.9.2 Input Data 33
3.9.3 Output Data 34
3.9.4 Mathematical Statement 34
3.9.5 Accuracy 36
References 37
Appendix A. **Acronyms 38**

Table of Figures

FIGURE 1: INTERFACE DIAGRAM 10
FIGURE 2 FLOW DIAGRAM OF THE LEVEL 1 HR SLC PROCESSING STEPS USED TO GENERATE THE L1B_HR_SLC PRODUCT. 11

Table of Tables

TABLE 1. HIGH LEVEL DESCRIPTION OF THE FUNCTIONS USED TO GENERATE THE L1B_HR_SLC PRODUCT 10
TABLE 2 DOPPLER ESTIMATION ERROR OVER LAND (THE VALUES OF COLUMNS REFERENCE, ESTIMATED AND DIFFERENCE ARE THE RATIO OF THE DOPPLER TO THE PRF AND NORMALIZED TO 2π) 20
TABLE 3 POINT TARGET HEIGHT ERRORS 32
TABLE 4 POINT TARGET ALONG TRACK ERRORS 33

List of TBC Items

Page	Section

List of TBD Items

Page	Section

1 Introduction

1.1 Purpose

The purpose of this Algorithm Theoretical Basis Document (ATBD) is to describe the physical and mathematical basis for the science data processing algorithms that are used to generate the SWOT Level_1B_HR_SLC (High Rate Single Look Complex) science data product. These algorithms are applied in the L1B_HR_SLC science algorithm software (SAS). The L1B_HR_SLC SAS performs Level 1 processing of the telemetry data from the SWOT KaRIn (Ka-Band Radar Interferometor) system. This document describes the Level 1 processing steps and their corresponding algorithm theoretical basis.

These algorithms and the associated SAS are used to create both the shorter latency and the standard latency versions of the HR_SLC products. The short latency version of the product uses the medium-precision orbit ephemeris (MOE) products, while the standard latency version of product requires the precise orbit ephemeris (POE).

1.2 Scope

The scope of this document is to:

1. Identify the list of primary functions that compose the processing steps within the SAS_L1B_HR_SLC SAS and their flow. These functions are broken down by the primary functional steps involved in the processing.
2. Describe the purpose of each of the functions.
3. Describe the input data to each function.
4. Describe the output data from each function.
5. Describe the mathematical basis of the algorithm in each function.
6. Describe the expected accuracy and/or limitations of the algorithm in each function.
7. Provide the relevant references for the algorithms described in this document.

1.3 Document Organization

Section 1 provides the purpose and scope, of this document.

Section 2 provides the background and context of the algorithms described in this document, and the functional flow of the primary functions (e.g., block diagram).

Section 3 provides the algorithm description for each of the functions shown in the block diagram, including input data, output data, mathematical basis, and expected accuracy.

Section 4 provides references for the algorithms described in this document.

Appendix A provides a listing of the acronyms used in this document.

1.4 Citing This Document

Please cite this document as follows:

> JPL D-105503, “SWOT Algorithm Theoretical Basis Document: Level 1B KaRIn High Rate Single Look Complex Data (L1B_HR_SLC) Science Algorithm Software,” Jet Propulsion Laboratory Internal Document, 2023.

2 Overview

2.1 Background and Context

The Surface Water and Ocean Topography (SWOT) mission is a partnership between two communities, physical oceanography and hydrology, to share high vertical accuracy topography data produced by the payload, whose principal instrument is the Ka-band Radar Interferometer (KaRIn). The details of SWOT mission objectives and requirements can be found in the SWOT Science Requirements Document [1]. The broad scientific goals can be summarized as follows:

Oceanography: characterize the ocean mesoscale and submesoscale circulation determined from the ocean surface topography at spatial resolutions of 15 km (for 68% of the ocean).

Hydrology: To provide a global inventory of all terrestrial surface water bodies whose surface area exceeds $(250m)^2$ (goal: $(100m)^2$, threshold: $1km^2$) (lakes, reservoirs, wetlands) and rivers whose width exceeds 100m (goal: 50m, threshold: 170m). To measure the global storage change in terrestrial surface water bodies at sub-monthly, seasonal, and annual time scales. To estimate the global change in river discharge at sub-monthly, seasonal, and annual time scales.

This document describes the Level 1 processing steps that are used to generate the L1B_HR_SLC science data product from input data which includes the L0B_HR_Frame, INT_KCAL_Dyn, MOE/POE, ATTD_RECONST and other auxiliary and ancillary data. The purpose of L1B_HR_SLC product is to provide high resolution single look complex (SLC) images and their corresponding radiometric calibration X factors for converting the SLC images into sigma0 images. The L1B_HR_SLC products are available mostly over land, as defined by the HR mask. A description of the L1B_HR_SLC science data product is provided in [2].

2.2 Functional Flow

*Figure **1*** shows the interface diagram of the L1B_HR_SLC processor. *Figure **2*** illustrates the flow of the processing steps within the PGE_L1B_HR_SLC processor. Table 1 provides a high-level description of each of the processing functions that are used to generate the L1B_HR_SLC product.

The SWOT KaRIn instrument collects data from both left and right side of the flight track. The algorithms described here are applied independently to the data collected from either side. As long as all the input data are available, the algorithms can be applied to any output tile in any order.

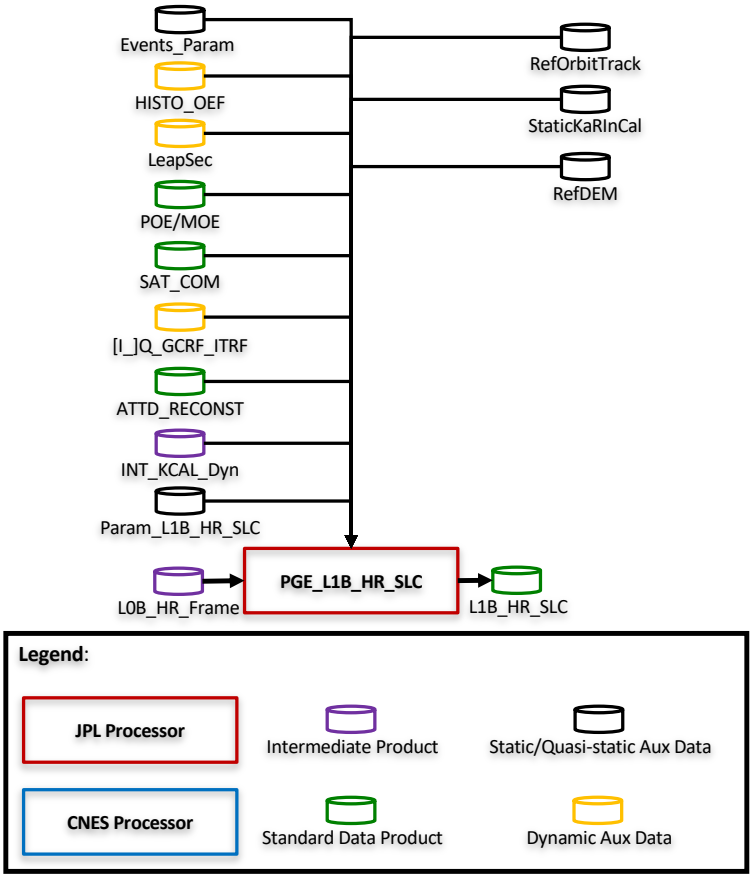

Figure 1: Interface Diagram

Table 1. High level description of the functions used to generate the L1B_HR_SLC product

Function Name	Description
Generate TVP file	Generate tvp file from input Events_Param, Histo_OEF, LeapSec, MOE/POE, ATTD_RECONST, [I_]Q_GCRF_ITRF, SAT_COM, and StaticKaRInCal.
extract range reference function	Extract the range reference function and other dynamic radar system parameters from StaticKaRInCal and INT_KCAL_Dyn.
range_compression	To resolve data in range with range resolution of about 0.75m.
Doppler_centroid_estimation and attitude correction	(Optional) Estimate the Doppler centroid based on the range compressed data and the estimated residual Doppler centroid will be used for attitude correction.
Generate GrDEM	Generate GrDEM, which is a local ground-range digital elevation model based on the input reference DEM and platform information of TVP.
Calculate_image_grids	Define the 3D reference geolocation of each of the SLC image grid samples based on zero Doppler geometry and the input reference DEM.
Determine sensor illumination time	For each image grid sample, determine the sensor illumination time/position so that the target at that image grid sample is illuminated by the antenna azimuth peak from that sensor position.
Azimuth compression	Azimuth compression using time-domain back-projection for each of the image grid samples.
Radiometric calibration	Calculate the radiometric calibration X factor, with which the sigma0 of each image pixel can be derived.

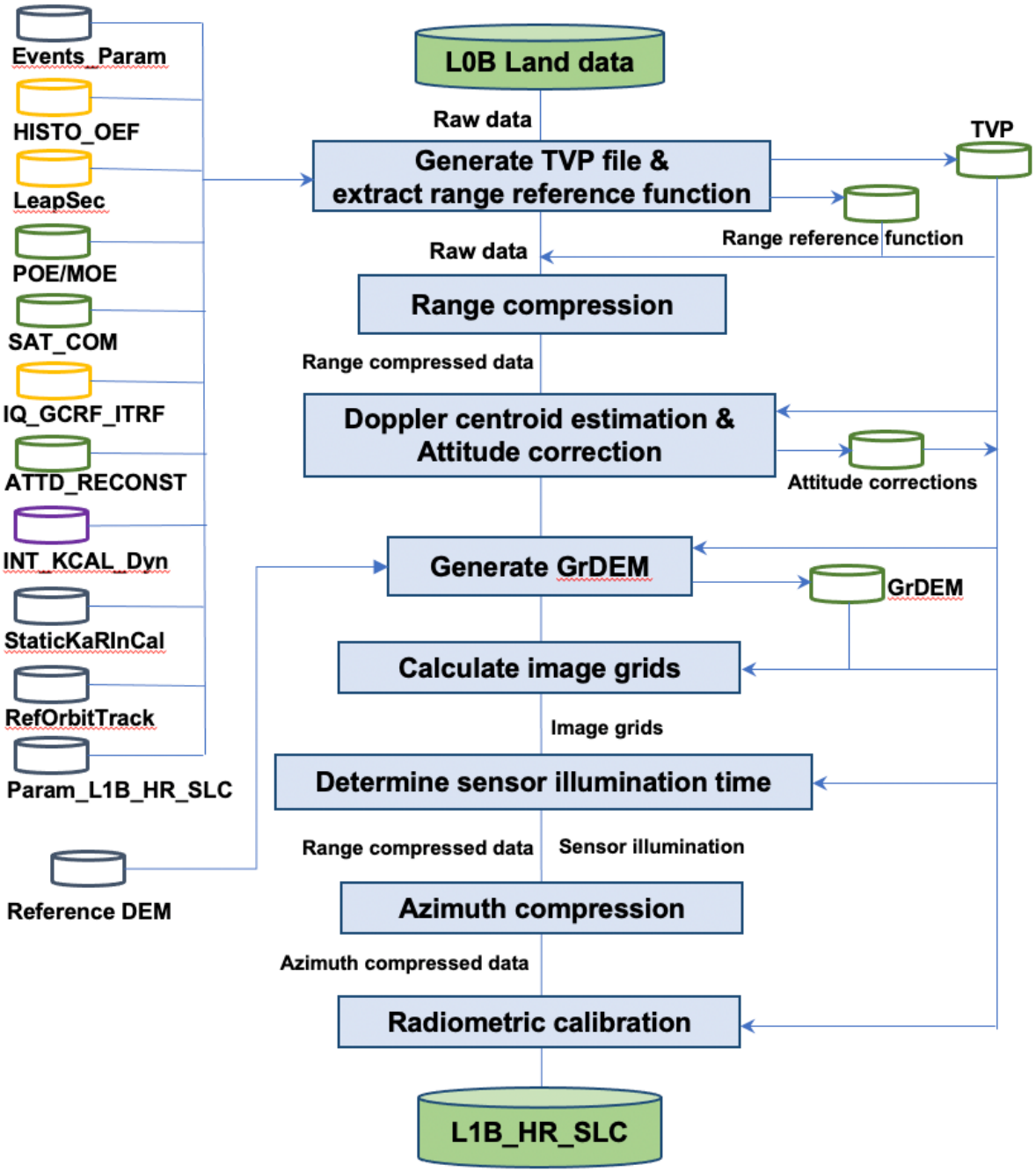

Figure 2 Flow diagram of the Level 1 HR SLC processing steps used to generate the L1B_HR_SLC product.

3 Algorithm Descriptions

3.1 Generate TVP file

3.1.1 Purpose

Generate the Time Varying Parameters (TVP) to cover the input raw data. As is described in Section 3 of the product description document [2], the L1B_HR_SLC product is organized into overlapping, swath-aligned tiles. Without overlap, each tile would be approximately 64 km in along track and would cover half of the SWOT swath (left or right) for about 64 km in cross track. With an additional 4 km on each end of the tile for overlap used by downstream product generation, the total along-track length of each SLC tile is approximately 72 km. To produce the 72 km SLC image of a tile, extra raw data at each end of a tile are needed to account for the synthetic aperture and possible squint geometry of the antenna pointing. The attitude of the SWOT spacecraft will be controlled so that the 1-sigma pitch will be 0.033^{O}. The antenna beam width after presumming is about 0.05^{O}. Therefore the total squint angle will be less than $0.033^{o} + 0.05^{O} = 0.083^{O}$, which corresponds to about 1.25 km along the track. Considering both ends of a tile, the total raw data extent is about 72 km + 2 x 1.25 = 74.5 km.

The TVP parameters are functions of time and include platform geolocation, velocity and attitude information and the antenna coordinates. There will be one set of these parameters for each of the radar pulses. (Note that KaRIn implements on-board presumming by a factor of 2.125, so individual echoes available during ground processing do not coincide with actual transmitted pulses; however, the term “pulses” is nevertheless used in this document to refer to the presummed echoes, with additional explanation only when the context is insufficient to avoid confusion.) The nominal distance the sensor travels between two successive pulses is about 2.9 m for the presummed raw data. For a tile of 74.5 km long in along track, we will have about 25700 pulses and thus 25700 values for each TVP parameter. The TVP parameters will be saved into the SLC product and will be used also in the later processing stages. A complete description of TVP product is given in L1B_HR_SLC product description document [2].

3.1.2 Input Data

Description	Source
Satellite events files to provide the times when spacecraft events occur.	HISTO_OEF
Events parameters to provide parameters related with the HISTO_OEF data handling.	Events_Param
Leap Second data to provide the leap seconds between the UTC time and the TAI time	LeapSec
Translation between the spacecraft center of mass and the origin of the KMSF reference frame so that the KMSF origin	SAT_COM
Medium-precision orbit ephemeris / precise orbit ephemeris to provide the geolocation and velocity information of the mass center of the KaRIn Mechanical System Frame (KMSF)	MOE/POE
Attitude of KMSF	ATTD_RECONST

Rotation (as a quaternion) between the inertial reference frame (GCRF) and the Earth-fixed reference frame (ITRF) so that the attitude of the KMSF reference frame can be determined from the ATTD_RECONST data, which give spacecraft attitude relative to the inertial frame.	[I_]Q_GCRF_ITRF
Static KaRIn Calibration to provide leverarm relative postion with respect to the KMSF center	StaticKaRInCal

3.1.3 Output Data

Description
TVP parameters at the time when each pulse is transmitted. The nominal PRF after presum is about 2000 Hz. Both the UTC and TAI times are given in seconds since beginning of year 2000 for each set of the TVP parameters. Within SLC processor, TAI time is always used.
X, Y, Z coordinates of the KMSF origin in ECEF frame
Vx, Vy, Vz of the KMSF origin in ECEF frame
Attitude (roll, pitch and heading) of the KMSF frame
Antenna position for each of the two interferometric antennas in ECEF frame

3.1.4 Mathematical Statement

The TVP parameters are defined with respect to a KaRIn-fixed frame called KMSF (KaRIn metering structure frame). The precise definition of this frame is somewhat arbitrary provided that the frame remains fixed to the KaRIn instrument and that other parameters are consistently defined with respect to this KaRIn-fixed reference frame.

All the TVP parameters are given from our input with some time intervals. What is done in this function is to interpolate each of the TVP parameters at a time interval of the PRI (pulse repetition interval, on the order of 0.5ms) of the KaRIn system. All the interpolations, including KMSF center position coordinates, velocity vectors, antenna position coordinates, ATTD_RECONST, [I_]Q_GCRF_ITRF quaternions and the rotation matrics defined by both ATTD_RECONST and [I_]Q_GCRF_ITRF quaternions, are done by using GECO (software package developed by CNES). The position and velocity interpolations are done with Everett interpolations and the quaternion and rotation matrix interpolation are done with Spherical Linear Interpolation. The details are described in [3]. The interpolated rotation matrics are then converted into the roll, pitch and yaw attitude angles.

3.1.5 TVP Parameter Interpolation Accuracy

The interpolation accuracy is better than one micro-meter for position and better than one micro-meter per second for velocity as shown in the GECO documents [3].

3.2 Extract range reference function

3.2.1 Purpose

A range reference function is required for range compression in the SLC processor. The ideal range reference function is the replica of the transmit chirp. The KaRIn system records the transmitted chirp in its L0B_Cal_Frame data and in 300 MHz sampling frequency.

The downlinked cal-chirps can be used directly as the range reference functions for the down stream range compression. However, the nosie contained in the cal-chirps will contribute some SNR decrease in the range compressed data. To improve the quality of the reference chirps, we will process the downlinked chirps offline and averaging enough data from the calibration phase of the mission to produce static reference functions with negligible noise. These processed chirps are provided to the SLC processor in the StaticKaRInCal auxiliary input file. There are all together 17 different chirps depending on the pulse duration. One of the 17 chirps will be used as the base reference chirp for one pulse of echo data. The chirp phase drift between the downlinked cal-chirp and the recorded base reference chirp are determined in the dynamic calibration processor such that a modified based reference chirp will eventually be used for range compression.

The original chirps, including the cal-chirps and the base chirps, are I/Q sampled at 300 MHz. The echoes are also received first in 300 MHz sampling frequency and re-sampled with the 200 MHz sampling frequency in the On-Board-Processor (OBP) before downlinking.

3.2.2 Input Data

Description	Source
Dynamic Calibration product to provide calibrated transmit chirp	INT_KCAL_Dyn

3.2.3 Output Data

Description
Range reference function (calibrated transmitted chirp)

3.2.4 Mathematical Statement

Two different processes are used to produce the range reference function for the echo data: (1) generate 17 base reference chirps for the 17 different pulse durations; (2) produce the final reference chirp from the downlinked cal-chirp and the corresponding base reference chirp. The first process only needs to be done once offline when we generate the StaticKaRInCal product and before the SLC processor is used. We describe its mathematical formulation here briefly as a reference.

Let’s assume that there are N downlinked chirps for the same pulse width: ch(n, k), with n = 0,1, 2, …, N-1 and k = 0,1,2, …, K-1. N is the total number of used chirps with the same

pulse width and K is the total samples for each chirp where K = pulse_width * sampling_freq, with a typical pulse width of 6.4 μs and sampling frequency of 300 MHz yields a K of 1920 complex range samples. We produce one averaged chirp out of the N chirps. We expect the chirps to be very stable over the time, but the algorithm accommodates a small phase drift between the successive chirps.

The steps used to produce the averaged base chirp:

(1) base_ch(k) = ch(0, k), k = 1,2,…, K-1;
(2) For n = 1,2, …, N - 1
base_ch(k) = base_ch(k) + ch(n, k) * exp{-jα_n}, with

$$\alpha_n = \arg\{\sum_{k=0}^{K-2} ch(n,k) * conj[base\_ch(k)]\}$$

The averaged chirp is saved as base reference chirp for all land frame data in the StaticCal product.

When processing the land frame data, we use these recorded base reference chirps and the corresponding cal-chirps associated with the echo. A similar process is used to produce the final reference chirp ref_ch() as follows:

(1) Determine the phase drift for chirp n: $\alpha_n = \arg\{\sum_{k=0}^{K-1} ch(n,k) * conj[base\_ch(k)]\}$
(2) Calculate the final reference chirp: ref_ch(k) = ch(n,k)*exp{jα_n}, k = 0,1,…, K-1.

The final reference chirp is still at a 300 MHz sampling frequency and needs to go through a re-sampling process to be resampled down to the the raw signal sample rate of 200 MHz. The same 3rd band Nyquist filter with a filter length of 99 and a Hamming weighting, as used in OBP, is used for the low pass filtering and resampling. The detailed description of the re-sampling process can be found in KaRIn_OBP_land_ATBD [4].

3.2.5 Range Reference Function Accuracy

The accuracy of the range reference functions affects the final accuracy of the SWOT interferometry and will be addressed togother in section 3.8.5.

3.3 Range Compression

3.3.1 Purpose

The L0B HR data is framed telemetry raw data received by our ground stations. It is the echo response of the targets, including terrestrial water bodies like lakes and rivers, vegetated wet land and general terrestrial land, to the transmitted signal, which is a chirp or a linear-frequency-modulated pulse waveform. The chirp's pulse duration is nominally 6.4 μs and the chirp's signal bandwidth is 200 MHz. For each pulse of the received data, the energy received for each target scatterer is determined by the transmitted waveform and the propagation delay of the waveform through the atmosphere to the target and back to the receiving antennae. The energy from scatterers is spread out in many samples of each pulse, depending the pulse

duration and the sampling frequency.

The purpose of range compression is to gather the energy received during multiple samples into a single point, so that after range compression the targets are well resolved in range.

3.3.2 Input Data

Description	Source
L0B Land raw data	L0B Land
Range reference function	Output of extract range reference function
Range weighting	Specified in the processing parameters

3.3.3 Output Data

Description
Range compressed data

3.3.4 Mathematical Statement

The range compression is done pulse by pulse by using matched filter or cross correlation of the echo with the transmitted signal, which we call the range referene function. It is achieved by convolving the received signal with a conjugated and time-reversed version of the reference function. This time-domain convolution is implemented with frequency-domain multiplication as follows to gain computational efficiency.

Let's assume the received echo is f(p, n), where p is the pulse index and n is the range sample index. There are total N sampled received for the pulse. The range reference function is h(p, m) with m = 0, 1, 2, …, M-1, total M samples. We use N_{fft} (>= N+M) to represent the FFT length we will use to do Fast discrete Fourier Transformation (FFT) on the echo and the reference function. In order to use an efficient FFT algorithm, N_{fft} needs to be a number of power of 2. Let F(p, k) be the discrete fourier transformation of echo $f(p, n)$ and H(p, k) be the discrete fourier transformation of the range reference function h(p, m).

To preserve fine range resolution (and hence looks in downstream processing) as much as possible, the SWOT SLC processor does not use any range weighting. Note that the SWOT measurement is geared toward water surfaces, which are typically much brighter than land surfaces at SWOT incidence angles, so the poor integrated sidelobe ratio (ISLR) associated with the lack of spectral tapering does not unduly affect the measurement. The range weighting can be applied for debug and other purposes. It takes the forms of raised cosine function:

$$W(k) = a_0 + (1 - a_0) \cdot \cos\left(\frac{2\pi k}{N_{fft}-1}\right), \text{ where } a_0 >= 0.5, \text{ and } k = 0, 1, \ldots, N_{fft}-1 \qquad (1)$$

In the case of no weighting, W(k) = 1 for k = 0, 1, …, N_{fft}-1. Multiplying the DFT of the echo with conjugate of the DFT of the reference function and the weighting W(k), we get the DFT of the DFT $F_{rc}(p, k) = W(k) \cdot F(p, k) \cdot H^*(p, k)$ of the range compressed data $f_{rc}(p, n)$, which can be obtained by doing inverse DFT of $F_{rc}(p, k)$.

In the downstream processing, time-domain back-projection will be used for azimuth compression. The time-domain interpolation of the range compressed data is the major

operation involved in back-projection algorithm. The accuracy of this interpolation depends on the frequency spectrum structure of the range-compressed data. The KaRIn system uses a sampling frequency of 200 MHz for the downlinked raw data with a final bandwidth very close to 200 MHz. Since the signal bandwidth to the sampling frequency ratio is very close to one, any interpolation algorithm produces error due to the non-perfect frequency response of the interpolator. In order to reduce the interpolation errors, we over-sample the range compressed data by a factor of 2. This over sampling operation is done in the frequency domain by extending the spectrum $F_{rc}(p, k)$ by a factor of 2, i.e., by zero-padding the added high frequency bins before the inverse DFT (see Figure 3).

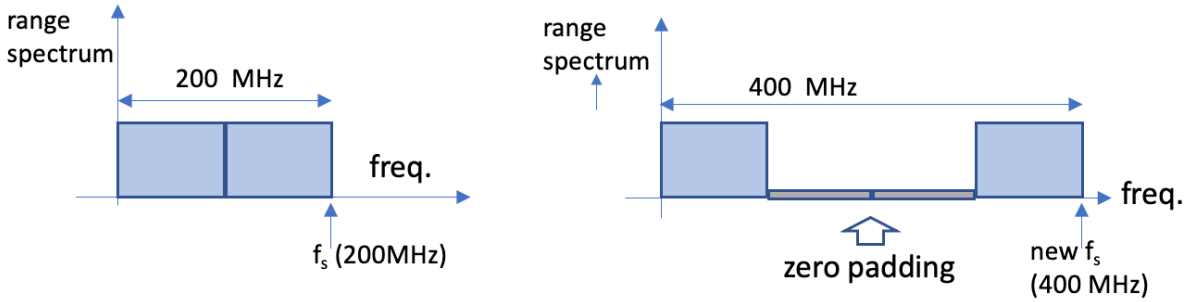

Figure 3. illustration of zero padding the high frequency sampling bins with doubled sampling frequency.

3.3.5 Range Compression Accuracy

The accuracy of the range compression will be addressed togother in section 3.8.5.

3.4 Doppler Centroid Estimation and Attitude correction

3.4.1 Purpose

The Doppler or Azimuth frequency modulation of the returned signal is determined by the projection of the platform velocity onto the line of sight to the targets, which is largely determined by the attitude of the radar antennas and altitude of the radar platform. In order to properly focus the images and not introduce biases in the surface height estimation, the platform attitude and orbit parameters must be known with significant accuracy. If the platform attitude information provided is accurate enough we can directly use it. In case the accuracy of those ephemeris measurements is not sufficient, improved estimates must be made from the data itself. The SWOT KaRIn system does Doppler centroid estimation on board and uses the estimated Doppler centroid to base-band the along track data spectra before presumming, an along track down sampling process to reduce the data volume. (Parameters describing the Doppler term that is removed during on-board processing are also downlinked; this information is used during ground processing to recover the original echo phase.) The on-board estimated Doppler information is downlinked and we can choose to use it directly or re-estimate it in the ground processing stage. The final decision of whether to (1) use the provided platform attitude, or (2) use the on-board estimated Doppler, or (3) re-estimate Doppler on the ground will be made after we have evaluated the quality of the ephemeris data. The following

describes how the re-estimation of the Doppler centroid is done within the SLC processor and how the Doppler centroid estimates are converted into attitude corrections.

Because of the discrete sampling of data in the along-rack direction, an estimate of the Doppler centroid is ambiguous. Thus, the estimate of the Doppler centroid is typically broken into two parts, the fractional part and an integer ambiguity part. The Doppler estimation described here is to estimate the fractional part. The ground-reconstructed attitude will be sufficient to estimate the correct ambiguity, i.e., is better than ½ a KaRIn azimuth beamwidth.

3.4.2 Input Data

Description	Source
Range compressed data	L1B_SLC_processor
TVP	ATTD_RECONST and POE / MOE
L0B Land data	L0B_Land_frame
L0B Dynamic Calibration data	INT_Dyn_Cal

3.4.3 Output Data

Description
Refined range and time dependent Doppler centroid and estimated corresponding attitude correction

3.4.4 Mathematical Statement

The SWOT OBP provides on-board Doppler estimation. The estimated Doppler information is downlinked through the L0B Cal data frames. The on-board Doppler estimation theoretically should produce better accuracy since the estimation is based on the raw data with the original PRF of about 4420 Hz. The L0B land data are sampled with reduced PRF of about 2000 Hz after presumming with a presumming factor 2.125 or 2.4375. In the case that the POE/MOE and ATTD_RECONST provided platform attitude is not accurate enough and the SWOT OBP Doppler estimator does not work as well as expected, then re-estimation of Doppler is needed during SLC processing.

We use the same Doppler estimation method, time-domain pulse-pair Doppler centroid estimator, used in the [4]. A description of this method can also be found in section IV of [5]. Since KaRIn is almost nadir looking, the Doppler centroid is sensitive mainly to pitch and remains nearly constatnt within the 50 km swath width from near to far range. Because the radar antenna pointing variation is a slowly varying function of time, we can also assume that the Doppler centroid is constant within the 10 second duration of one tile (64 km long). Therefore, we only make one Doppler centroid estimate for each tile.

The KaRIn observes both left and right swath with two pairs of interferometric antenna. The echos received from the antenna of each side are recorded into their corresponding channels refered to as reference (transmitting and receiving) and secondary (receiving only) denoted as ref and sec, respectively in the following. The Doppler estimation is then expressed as:

$$\widehat{f_D} = \frac{PRF}{2\pi} arg\{\sum_{n,k}\{h_{ref}(n+1,k)\cdot {h_{ref}}^*(n,k) + h_{sec}(n+1,k)\cdot {h_{sec}}^*(n,k)\}\} \quad (2)$$

where $\hat{f}_D$ is the Doppler estimate, n represents a pulse index and k a range bin of the range compressed reference channel data $h_{ref}(\cdot)$ and secondary channel data $h_{sec}(\cdot)$, and PRF is the pulse repetition frequency. Since the platform data provide us a very good Doppler centroid prediction, we can estimate the residual Doppler centroid instead by:

$$\widehat{rf_D}(n) = \frac{PRF}{2\pi} arg\left\{\sum_{n,k}\{h_{ref}(n+1,k)\cdot {h_{ref}}^*(n,k) + h_{sec}(n+1,k)\cdot {h_{sec}}^*(n,k)\} \cdot exp\left\{-\frac{2\pi Dc_{pred}}{PRF}\right\}\right\} \quad (3)$$

where Dc_{pred} is the predicted Doppler centroid using the POE/MOE and ATTD_RECONST provided platform data and the $\widehat{rf_D}(n)$ is the residual Doppler centroid estimate. The final estimated Doppler centroid will be $\widehat{f_D}(n) = Dc_{pred} + \widehat{rf_D}(n)$. Since the Doppler centroid is mainly sensitive to pitch for SWOT geometry, the Doppler frequency f_D is mainly dependent on pitch:

$$f_D = 2\frac{\vec{v}\cdot\hat{\vec{l}}}{\lambda} = 2\frac{v\cdot sin\theta_p}{\lambda}, \quad (4)$$

where v is the sensor velocity, λ is the signal wavelength, θ_p is the pitch angle. Taking a derivative on both sides, we get:

$$df_D = 2\frac{v\cdot cos\theta_p}{\lambda}\cdot d\theta_p \approx \frac{2v}{\lambda}\cdot d\theta_p. \quad (5)$$

Rearranging Eq.(5), we have $d\theta_p \approx \frac{\lambda}{2v}\cdot df_D$. And therefore the pitch error is related to residual Doppler centroid by:

$$\theta_{pitch\_corr} = \frac{\lambda}{2v}\widehat{rf_D} \quad (6)$$

where v is the platform velocity. This pitch correction together with the platform roll, pitch and yaw measurements is used to calculate the antenna peak pointing for SLC processing.

3.4.5 Doppler Centroid Accuracy

The accuracy of data based Doppler estimation depends mainly on the SNR of the data and on the homogeneity of the scene over the 10 second estimation interval. Land SNR is significantly lower than water SNR and for most areas the land SNR is less than zero dB. Note also that the water surface regions, not including the ocean, covers less than 10% of the total land area. In order to address the Doppler centroid estimation accuracy, we have simulated 10

land tiles from the California coast to northern Canada, where the water coverage is much less than 10% of the simulated land areas. The truth DEM used for simulation has roughly 250m resolution and is part of GMTED (Global Multi-resolution Terrain Elevation Data), which is the integrated result of global Digital Terrain Elevation Data (DTED) from the Shuttle Radar Topography Mission (SRTM), Canadian elevation data, Spot 5 Reference3D data, and data from the Ice, Cloud, and land Elevation Satellite (ICESat). The reference DEM used for SLC processing and Doppler estimation for this analysis was an averaged version of the SRTM DEM with a resolution of roughly 900m. (Note that the reference DEM for SWOT operational processing will have much finer resolution, however.) Table 2 shows the peak SNR of each tile and the truth Doppler, the estimated Doppler and the Doppler estimation error (Doppler difference) for the 10 tiles, where the Dopplers are normalized to cycles by dividing by 2π and the peak SNR is calculated from the raw echo data, and the raw data SNR is calculated using averaging over 1000 range bins and 70km long azimuth data lines: SNR = S/N, where S is the singal power and N is the noise power. These 10 tiles are all from ascending passes starting from the California coast and heading towards Canada. The best case is CA_p1 left swath with peak SNR of 1.6772 dB, where the Doppler error is -0.03394 (units), which corresponds to $0.03394/2\pi = 0.54\%$ of the PRF. The worst case is CA_6 right swath with peak SNR of -9.142 dB, where the Doppler error is 0.3092, which corresponds to $0.3092/2\pi = 4.92$ % of the PRF.

Table 2 Doppler estimation error over land (the values of columns reference, estimated and difference are the ratio of the Doppler to the PRF and normalized to 2π)

Scene	Left Swath				Right Swath			
	Peak SNR	Reference	estimated	difference	Peak SNR	Reference	estimated	difference
CA_p1	1.68 dB	-8.28	-8.32	-0.034	0.57 dB	-8.27	-7.98	0.29
CA_p2	-4.85 dB	-8.55	-8.65	-0.103	-4.56 dB	-8.53	-8.35	0.18
CA_p3	-7.10 dB	-8.79	-8.74	0.051	-6.68 dB	-8.78	-8.60	0.18
CA_p4	-3.92 dB	-8.93	-8.96	-0.029	-2.25 dB	-8.91	-8.72	0.19
CA_p5	-9.44 dB	-9.06	-8.97	0.094	-10.44 dB	-9.04	-8.81	0.23
CA_p6	-5.04 dB	-9.14	-9.07	0.074	-2.08 dB	-9.14	-8.83	0.31
CA_p7	-5.18 dB	-9.17	-9.07	0.103	-2.62 dB	-9.15	-8.94	0.21
CA_p8	-6.26 dB	-9.16	-9.38	-0.23	-7.63 dB	-9.14	-8.89	0.26
CA_p9	-10.21 dB	-9.11	-9.25	-0.14	-7.70 dB	-9.09	-9.19	-0.095
CA_p10	-0.081 dB	-9.00	-8.94	0.056	-0.59 dB	-8.98	-8.78	0.20

3.5 Generate GrDEM

3.5.1 Purpose

The time-domain back-projection approach used for forming the SLCs requires the geo-reference location for each image pixel. The reference locations are used to focus the image, to coregister the two interferometric images from two interferometric channels, and to phase

flatten the interferogram formed from the reference and secondary SLCs in the downstream Pixel Cloud processing.

In order to have, easily accessable and continiuos geo-references, even across the tile boundaries, we define the two dimensional Ground range DEM (GrDEM). The first dimension is the row which is aligned with the sensor's along track, and the second dimension is the column, which is aligned with the cross-track direction that is perpendicular to the local ground projected velocity. The along-track spacing between rows is not exactly uniform because it is tied to and decimated from the TVP sampling. The decimation factor is chosen to approximately match the reference DEM resolution. The cross track spacing between the columns is chosen as a constant, which also matches the reference DEM resolution.

3.5.2 Input Data

Description	Source
Reference DEM	Static priori DEM database
TVP	ATTD_RECONST and POE / MOE

3.5.3 Output data

Description
GrDEM

3.5.4 Mathematical Statement

The input TVP file provides state vector of the KaRIn frame at each of the transmitting pulses. Therefore, we have the time, location P(x, y, z) in geocentric coordinates or latitude, longitude and altitude, and the velocity V(v_x, v_y, v_z) for each transmit pulse. The input reference DEM will be a mix of SRTM DEM and Multi-Error-Removed Improved-Terrain (MERIT) DEM. The DEM resolution will be between 30 and 90 meters. The spacing flown by the satellite between two successive pulses after presum is around 3 meters. To match the DEM ground resolution of 30 m or more, we undersample (decimate) the TVP parameters so that every few TVP pulses we take one sample in the along track direction for the GrDEM we are defining. The undersampling factor will be around 10 to match 30 m resolution. The cross track spacing for this DEM is specified independently and can be chosen to match to the input DEM resolution or to the groud range resolution of processed SAR image. For SWOT geometry, a typical cross track spacing is between 10 and 20 meters.

For each row of the GrDEM, we define a local cartesian coordinate system s-c-h, which is tangent to the Earyh ellipsoid at the first pixel in each row, where the s represents the along track, the c is the cross track and h is the height above the Earth ellipsoid. (Note that in other contexts, *s,c,h* coordinates refers to a spherical coordinate system, but here the coordinate system is cartesian and is redefined for each echo.) Let (λ, θ) be the geodetic latitude and longitude of the platform position and $\vec{v}$ the velocity vector in the geocentric coordinates. The nadir vector $\vec{n}$, which is locally perpendicular to the ellipsoid, is related to the geodetic latitude and longitude as follows:

$$\vec{n} = \begin{bmatrix} -cos\lambda \cdot cos\theta \\ -cos\lambda \cdot sin\theta \\ -sin\lambda \end{bmatrix} \quad (7)$$

The unit vector $\vec{h}$ is the negative of $\vec{n}$. The cross-track unit vector, $\vec{c}$, is given by the cross product of $\vec{h}$ with the velocity vector:

$$\vec{c} = \frac{\vec{h} \times \vec{v}}{|\vec{h} \times \vec{v}|} \quad (8)$$

The along-track vector, $\vec{s}$, is then given by:

$$\vec{s} = \frac{\vec{c} \times \vec{h}}{|\vec{c} \times \vec{h}|} \quad (9)$$

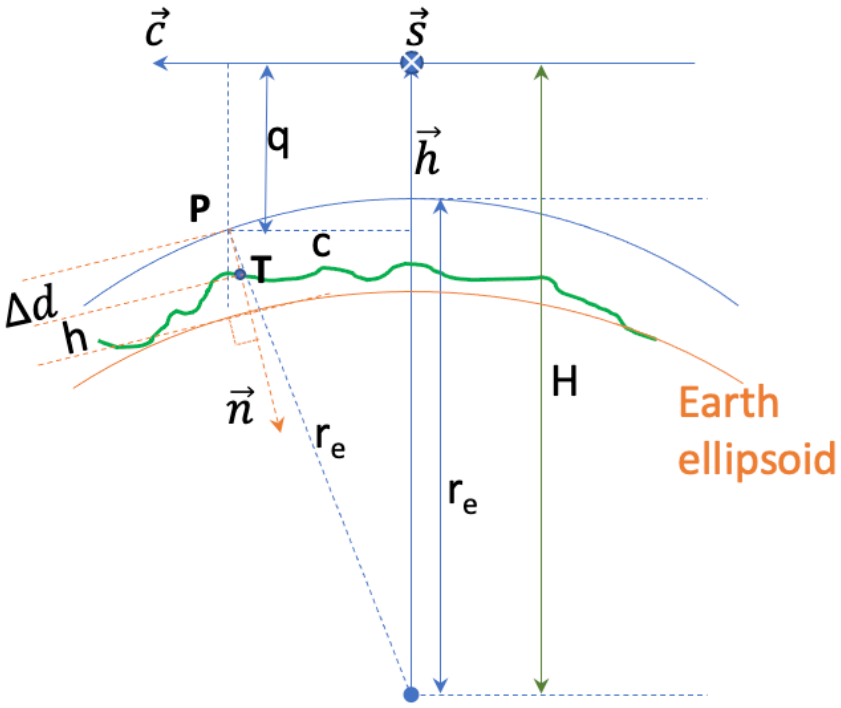

Figure 4 Local sch coordinate definition for GrDEM and relationships between GrDEM grid samples and their height above the Earth ellipsoid.

The c-h plane intersects with the Earth ellipsoid and the reference DEM (bold green curve) as shown in *Figure* . The along track vector $\vec{s}$ is pointing into the paper, the cross track vector $\vec{c}$ points to the left and the up $\vec{h}$ vector points up. Here r_e is the semimajor axis of the Earth WGS-84 ellipsoid. The semimajor axis is always used here, independent of where on the Earth the points are located. Let $\vec{S}$ be the origin of KMSF. A point $\vec{P}$ located on the spherical surface

of radius r_e and is given by the intersection point of the vertical line passing through $\vec{P}$ with cross-track coordinate c with the sphere of radius r_e:

$$\vec{P} = \vec{S} + c\vec{c} - q\vec{h} \tag{10}$$

where q = $\left(H - \sqrt{r_e^2 - c^2}\right)$ as shown in *Figure* 4. From the coordinates of $\vec{P}$ we can calculate its latitude and longitude, which are used to locate the position in the reference DEM and its corresponding height h above the Earth ellipsoid. The ellipsoid height h is measured along the local nadir vector $\vec{n}$ and is the distance between the intersection of the nadir vector $\vec{n}$ originating from the point P with the Earth ellipsoid and the intersection of $\vec{n}$ with the reference DEM at T.

In order to access the GrDEM, we save not only the height of each GrDEM grid sample but also its latitude and longitude. If we want to know the height for a certain coordinate (s, c), we find first the base grid sample coordinates s_i and c_i such that:

$$s_i \leq s < s_{i+1} \text{ and } c_i \leq c < c_{i+1} \tag{11}$$

And then perform a bilinear interpolation using the heights at (s_i, c_i), (s_{i+1}, c_i), (s_i, c_{i+1}), (s_{i+1}, c_{i+1}) to get the height at (s, c). If the latitude and longitude are also desired, a similar bilinear interpolation for latitude and longitude is used.

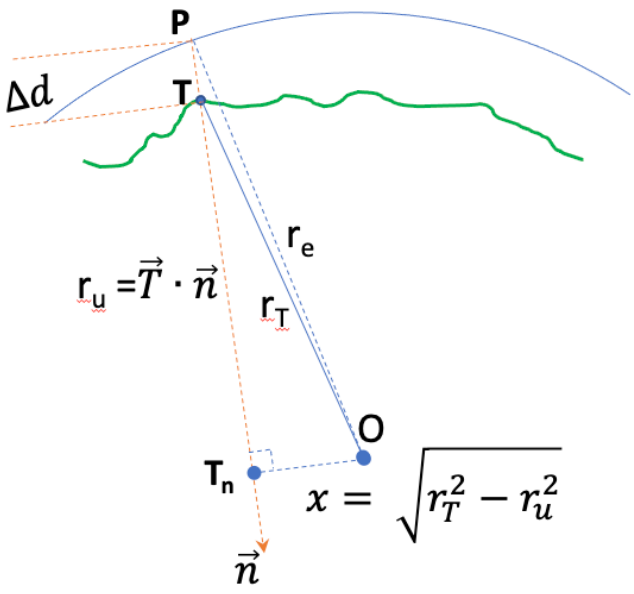

Figure 5. Relationships between nadir vector, sphere with radius r_e and point T on a DEM.

To determine the height on the GrDEM for a given point $\vec{T}$ with known latitude and longitude, we first find the corresponding point $\vec{P}$ on the sphere with r_e. Since point $\vec{P}$ and $\vec{T}$ have the same latitude and longitude, they have the same local nadir vector $\vec{n}$ and are related by

$$\vec{P} = \vec{T} - \Delta\mathrm{d} \cdot \vec{n} \tag{12}$$

where Δd is the distance between $\vec{P}$ and $\vec{T}$ as shown in *Figure 4*. Figure 5 exagerates the part around the point T so that the relationship between P, T and $\vec{n}$ can be better seen visually. O is the original of the Earth, T_n is the projection of vector $\overrightarrow{TO}$ onto the nadir vector. From figure 5, we have

$$r_u = \vec{T} \cdot \vec{n}, \tag{13}$$
$$x = \sqrt{r_T^2 - r_u^2}. \tag{14}$$

And the distance between P and T_n is:

$$\overline{PT_n} = \sqrt{r_e^2 - x^2} \tag{15}$$

Combining Eq. (11a), (11b) and (11c), we have

$$\Delta\mathrm{d} = \overline{PT_n} - r_u = \sqrt{r_e^2 + \left(\vec{T} \cdot \vec{n}\right)^2 - r_T^2} - \vec{T} \cdot \vec{n} \tag{16}$$

Using the $\vec{P}$ we can find the s-coordinate by making the look vector, starting from the platform position $\vec{S}$ to $\vec{P}$, perpendicular to the corresponding $\vec{s}$ vector, i.e.,

$$\left(\vec{P} - \vec{S}\right) \bullet \vec{s}(s) = 0 \tag{17}$$

The cross track coordinate c is the projection of the look vector onto the corresponding cross track vector $\vec{c}$:

$$c = \left(\vec{P} - \vec{S}\right) \bullet \vec{c}(s) \tag{18}$$

Using the known (s, c), we can get GrDEM height h(s,c) as described in the previous paragraphs.

3.5.5 GrDEM Accuracy

The GrDEM is a r epresentation of the topographic height information of the local target area. The accuracy of GrDEM will depend on the conversions between the GrDEM coordinates (row, col, height) and geodetic coordiantes (latitude, longitude, height) or coordinates (x, y, z) in earth-centered-earth-fixed system. We will not separately address its accuracy. Instead, the final height error, including GrDEM related errors, for both point targets and distributed targets will be presented in section 3.8.5.

3.6 Calculate Image Grids

3.6.1 Purpose

SAR images are a two-dimensional images. The time-domain back-projection method we use for azimuth compression gives us flexibility to define a reference 2D image grid, which is intuitive, convenient for use and helpful for downstream processing.

3.6.2 Input Data

Description	Source
GrDEM	L1B_SLC_processor
TVP	POE / MOE
L0B Land framed data	L0B_Land_frame

3.6.3 Output Data

Description
Image grid geolocation cooridnates in ECEF frame

3.6.4 Mathematical Statement

We chose the tangential velocity direction of the radar sensor as the one axis and the cross-track perpendicular to the tangential velocity as the other reference axis for each presummed pulse. The image grid samples are not uniformly spaced in either the along track and cross track directions. Instead we use a local reference DEM and the range between the sensor position at each presummed pulse and a surface point on the intersection of this reference DEM and the plane perpendicular to the leveled velocity direction. Since radar range resolution is the same for near range (even nadir looking) and far range, the ground range spacing is bigger near nadir and smaller for far range pixels for the same slant range spacing varying with the sine of the local incidence angle.

One reason we choose to define independent reference axes for each along track grid row is to avoid discontinuities between neighboring pulses at the tile boundaries. The SLC processor and SLC product are tile based. The downstream pixel cloud processing may need both the previous and the next SLC tiles for some averaging operations. If there is any systematic discontinuity between two neighboring tiles, errors would propagate to the pixel cloud products for the tile boundary pixels.

Figure 5 shows how the image grid samples in the cross-track direction are determined. For each presummed radar pulse, the local nadir pointing vector and the velocity vector defines the tangential cross-track direction for either the left or right side. The tangential along-track direction is defined by the cross-track direction and the down pointing vector. A sphere centered at the radar antenna of the reference (transmit) channel with radius r intersects the perpendicular plane at a circle on this perpendicular plane as shown in dashed lines. This circle has intersections with the reference DEM on each side of the swath (right side in the case of Fig. 6). For some near-range pixels, there might be no intersection between the iso-range circle

and the DEM. In such cases, we choose the intersections with the nadir-looking vector as the image grid samples. In the case of layover, the iso-range circle has more than one intersections with the DEM in which case we choose the one closest to nadir. The same set of reference locations are used for both interferometric SAR channels. Note that these locations are defined independent of the spacecraft attitude (the resulting slant-plane images are deskewed).

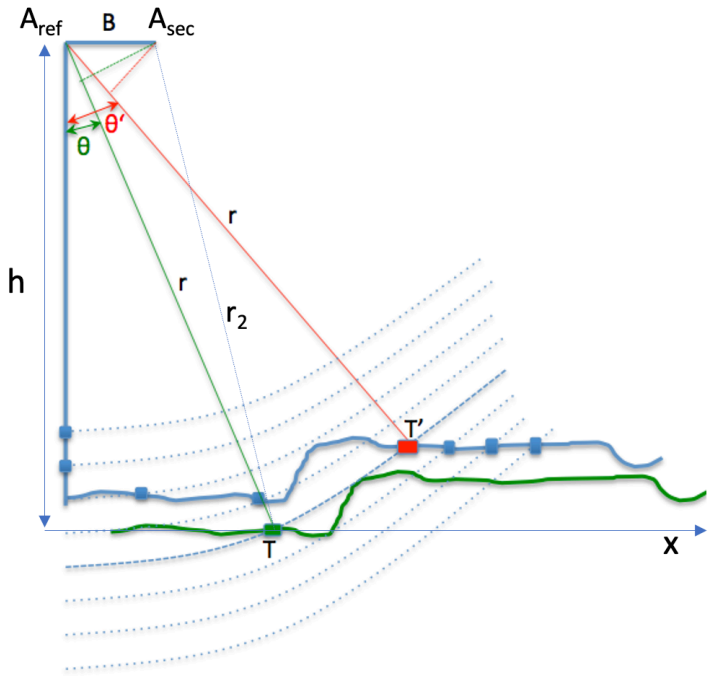

Figure 6 Slant range spacing for image grid. The blue squares denote the pixel locations on the reference DEM. The green line illustrates the actual surface.

3.6.5 Accuracy

The image grid coordinates are used as reference for 3 operations: SAR image focusing, image registration between the two interferometric channels, and interferogram phase flattening. The accuracy of the so determined along-track grid sample location is nearly independent of the quality of the reference DEM and is better than a pulse spacing (~3 m). However, the accuracy of the cross-track grid sample location is dependent on the reference DEM quality. An example is shown in Fig. 4, where the green curve represents the true DEM and the blue curve represents the reference DEM. For the same range r, the true location is T whereas T' would be used for processing.

The height error in the reference DEM will cause two main issues: (1) defocus of the image and (2) range registration error between the two interferometric channels. The description and calculation of the depth of focus for SAR can be found in the reference [6]. Using the formulas in [6], we can calculate the depth of SAR focus for SWOT geometry is better than 6 km, which is much bigger than the few tens of meters reference DEM height errors considered for SWOT.

The most strict requirement for a reference DEM is the image registration for the down stream interferometric processing after SLC processing. Using Fig. 4, we can get the range difference from target T to reference antenna A_{ref} and secondary antenna A_{sec} to be:

$$r - r_2 = \sqrt{h^2 + x^2} + \sqrt{h^2 + (x - B)^2} \tag{19}$$

where r is the distance between T and A_{ref} and r_2 is the distance between T and A_{sec}, h is the range altitude above the target, θ is the look angle, B is the baseline and x is the cross track. For a fixed range r, a height error dh will cause an error d(r-r2):

$$d(r - r_2) = -\frac{B}{x}\cos(\theta) \cdot dh \tag{20}$$

From a numerical analysis using SWOT parameters, for a DEM height error of 10m, we get about 5mm and 1mm range mis-registration at near range (10 km) and far range (60km), respectively. Those range mis-registration errors correspond to about 0.7% and 0.13% of the range resolution (0.75m) of the SAR image for near and far range pixels, respectively. Good image registration requires much smaller mis-registration error than 10% of the range resolution. Therefore, we do require a reasonably good reference DEM for SLC processing.

3.7 Determine sensor illumination position

3.7.1 Purpose

The SWOT platform with attitude control is very stable. Still it has non-zero roll, pitch and yaw and the platform changes its attitude slightly over time. Due to the non-zero platform attitude, the image grid samples on the same image line are not necessarily illuminated by the antenna azimuth peak from the same sensor position. In the SLC azimuth compression and downstream height reconstruction, the sensor illumination position for each image grid sample is required.

Not only does the SWOT patform have non-zero attitude, there might be some mounting errors between the antenna panels and the reference KMSF frame. These mounting errors can be estimated using the SWOT data over known flat topography areas with the calibration processor. In this section, we assume these antenna mounting errors are estimated already. We will describe the details of how we calculate the sensor illumination position for each image grid sample for non-zero attitude and non-zero attitude mounting error.

3.7.2 Input Data

Description	Source
Image grid samples	L1B_SLC_processor
TVP	L1B_SLC_processor, ATTD_RECONST and POE / MOE

3.7.3 Output Data

Description

Sensor illumination time and position (given as the index of the TVP array)

3.7.4 Mathematical Statement

The attitude of the spacecraft is an input to the processor. Although a best effort is made to align the antennas with the KMSF frame, there could still be some small mounting errors between each of the antennas and the KMSF frame. We use a set of rotation angles ($roll_a$, $pitch_a$, yaw_a) to represent the antenna face orientation with respect to the KMSF frame. Note that these parameters refer to a common rotation for both channels, as both must be processed to the same Doppler for interferometry. The antenna face is aligned with the KMSF face through a sequence of rotations $R_1(-roll_a)$, $R_2(-pitch_a)$, and $R_3(-yaw_a)$, where R_1 is the rotation about the first axis, R_2 is rotation about the second axis and the R_3 is rotation about the third axis. The antenna phase center coordinates in the KMSF coordinate system can be obtained by the following change of matrix operation

$$M_{ant}^{kmsf} = R_3(-yaw_a) \cdot R_2(-pitch_a) \cdot R_1(-roll_a) \tag{21}$$

where we assume the antenna panel rotational center is aligned with the KMSF center. The measured platform attitude parameters ($roll_p$, $pitch_p$, yaw_p) convert the KMSF coordinates into the standard earth fixed coordinate system TCN (Track, Cross track and Nadir) through the sequence of rotations:

$$M_{kmsf}^{tcn} = R_3(-yaw_p) \cdot R_2(-pitch_p) \cdot R_1(-roll_p) \tag{22}$$

The transformation from the antenna phase center's coordinates to the coordinates in the local TCN system is then:

$$M_{ant}^{tcn} = M_{kmsf}^{tcn} \cdot M_{ant}^{kmsf} \tag{23}$$

In the antenna face frame, the deflection vector (pointing in the along-track direction if aligned with KMSF) together with the elevation vector (pointing to the right side if aligned with KMSF) and the radiation vector (pointing along the the antenna boresight) form a right handed coordinate system. In this system, the unit vector $\overrightarrow{d_{ant}} = (1, 0, 0)^T$ becomes $\overrightarrow{d_{tcn}} = M_{ant}^{tcn} \cdot \overrightarrow{d_{ant}}$ in the local TCN system. If the look vector originated from the antenna phase center and pointing to the target is perpendicular to $\overrightarrow{d_{tcn}}$, the target is illuminated with the antenna peak in azimuth. The echo data received around that sensor illumination position represents the maximal energy that the target backscatters to the radar receiver and will be used to produce the focused radar image having the highest SNR. If we use T_{tcn}^{xyz} to represent the transformation from the local TCN frame to the Earth-centered-Earth-fixed corordinates, its unit vector in ECEF can be expressed as:

$$\overrightarrow{d_{xyz}} = T_{tcn}^{xyz}(\overrightarrow{d_{ant}}) \tag{24}$$

The illumination position for each image pixel can be easily found by a few iterations. Assume that the sensor position vector $\vec{S}(t)$ is a function of time, the corresponding velocity vector is $\vec{v}(t)$ and the image pixel position is $\vec{T}$. From the initial guessed illumination sensor position is $\vec{S}(t_0)$, we get the initial look vector $\vec{l}(t_0) = \vec{T} - \vec{S}(t_0)$. The projection of the look vector onto the antenna deflection vector is then $\vec{l}(t_0) \cdot \overrightarrow{d_{xyz}}(t_0)$ at the guessed sensor position. The time difference between the guessed position and the actual illuminating position is estimated as $\Delta t_0 = \vec{l}(t_0) \cdot \overrightarrow{d_{xyz}}(t_0) / |\vec{v}(t_0)|$. The new guess sensor position is $\vec{S}(t_0 + \Delta t_0)$. The same steps can be repeated until the time difference between the guessed position and new position is smaller than half of the PRI. Since the orbit trajectory is very smooth and is locally nearly linear within the 75 km long tile, this iteration approach is very effective and normally converges within 2 or 3 iterations.

3.7.5 Accuracy

The accuracy of the sensor illumination position is less than or equal to half the distance between two neighboring pulses by construction.

3.8 Azimuth Compression

3.8.1 Purpose

To generate azimuth and range compressed single look complex images and the radiometrically calibrated X factor images for both the interferometric channels with time-domain back-projection algorithm. The X factor provides the multiplicative conversion between engineering units and backscatter coefficient.

3.8.2 Input Data

Description	Source
Range compressed data	L1B_SLC_processor
Antenna patterns	Priori antenna pattern files
TVP	ATTD_RECONST, POE / MOE, StaticCal
Image grid	L1B_SLC_processor
Sensor illumination	L1B_SLC_processor

3.8.3 Output Data

Description
SLC images
Xfactor images

3.8.4 Mathematical Statement

The back-projection algorithm for SLC azimuth compression is a time-domain matched filter in the azimuth direction. In this method, each received radar echo is range compressed

first to resolve the targets in range, and then back projected over spherical shells to all the imaged pixels. Each image pixel is assigned a value by interpolating the range compressed pulse echo at the time delay corresponding to the range between the transmitting antenna and the image pixel plus the range from the image pixel and the receiving antenna. The value of each image pixel is the sum of all the echos within a specified azimuth antenna beam width.

Mathematically the back-projection algorithm can be described as

$$I(\vec{x}) = \sum_{|m-m_p(\vec{x})|<\Delta m(\vec{x})} w\left(m - m_p(\vec{x})\right) \cdot S\left(\tau\left(\vec{x}, \vec{p}(m), \overrightarrow{p_t}(\vec{x}, m)\right)\right) \cdot exp\{j2\pi f_c \tau(\vec{x}, \vec{p}(m), \overrightarrow{p_t}(\vec{x}, m))\} \quad (25)$$

where I is the SLC image, $\vec{x}$ is the image pixel position, m is the pulse index number, $m_p(\vec{x})$ is the pulse number corresponding to the center of illumination, which is described in section 3.7, $\Delta m(\vec{x})$, determined as follows:

$$\Delta m(\vec{x}) = \frac{\theta_{pbw} \cdot r\left(\vec{x}, \vec{p}(m)\right) \cdot PRF}{v} \quad (26)$$

is the number of pulses around the illumination pulse (position) so that the azimuth aperture forms the required processing beamwidth θ_{pbw}, $r\left(\vec{x}, \vec{p}(m)\right)$ is the average range between the target and the transmitting and receiving antennas, v is the platform velocity, PRF is the radar pulse repetition frequency, $\vec{p}(m)$ is the antenna position for receiving the pulse echo m , $\overrightarrow{p_t}(\vec{x}, m)$ is the transmitting antenna position for target located at $\vec{x}$, *w* is an apodization window, $S\left(\tau\left(\vec{x}, \vec{p}(m), \overrightarrow{p_t}(\vec{x}, m)\right)\right)$ is the interpolated range compressed data, and τ is a function describing the round trip time delay of the signal from the transmit antenna, to the pixel location and back to the receiving antenna. Back projection inherently fully compensates for the curvature of the orbit and attitude (and the Doppler centroid). No compensation for atmospheric delays is applied during SLC formation; corrections for such delays are handled in downstream processing. The operation specified in the above equation needs to be done for each image pixel $\vec{x}$. The number of pulses used for this integration is determined by the processing beamwidth and the distance between the image pixel location and the antenna location. The apodization window ***w*** is optional. A raised cos-function like described above for range compression can be used to reduce azimuth side lobes. The transmitting and receiving antenna impose a natural apodization through their antenna patterns. The antenna pattern apodization exists in the echo data $S\left(\tau\left(\vec{x}, \vec{p}(m), \overrightarrow{p_t}(\vec{x}, m)\right)\right)$. The echo received at the illumination position of a target has more weight and the weight on the echo is tapered down as the receiving position moves away from the illumination position. In some cases an extra apodization is not needed.

In a back-projection algorithm, there are two important operations. The first is to find the interpolated data $S\left(\tau\left(\vec{x}, \vec{p}(m), \overrightarrow{p_t}(\vec{x}, m)\right)\right)$ and the other is to compensate the phase $exp\{j2\pi f_c \tau(\vec{x}, \vec{p}(m), \overrightarrow{p_t}(\vec{x}, m))\}$ caused by the time delay $\tau(\vec{x}, \vec{p}(m), \overrightarrow{p_t}(\vec{x}, m))$. Both operations, especially phase compensation, need the time delay $\tau(\vec{x}, \vec{p}(m), \overrightarrow{p_t}(\vec{x}, m))$ precisely. To calculate the time delay we need to know all the 3 locations: $\vec{x}$, $\vec{p}(m)$, $\overrightarrow{p_t}(\vec{x}, m)$. We get

the target location $\vec{x}$ from the image grid sample, the transimitting antenna position $\overrightarrow{p_t}(\vec{x}, m)$ from the TVP array. However, the receiving antenna position $\vec{p}(m)$ is not explicitly known.

Fig. 7 shows the concept of how to take into account the delay between transmitting and receiving and to determine the receiving antenna position $\vec{p}(m)$. The platform moves along the velocity direction (from left to right). The radar transmits pulses along the track. After each pulse is transmitted the radar receives the echo. This process repeats pulse by pulse. The pulse transmitted at position $\overrightarrow{p_t}(m)$ travels the distance r_1 and reaches the target x. The reflected signal from target x travels distance r_2 and arrives at the antenna position $\vec{p}(m)$. In the meantime, the radar travels with the velocity $\vec{v}$ along the orbit and arrives at $\vec{p}(m)$ after a time delay of $\tau = s/v = \tau_1 + \tau_2$, where s is the distance traveled by the radar from $\overrightarrow{p_t}(m)$ to $\vec{p}(m)$.

We use $2\tau_1$ to approximate $\tau = \tau_1 + \tau_2$ and to determine the number of pulses in air n. Then we use quadratic interpolation to get an estimate of the $\vec{p}(m)$ from the 3 transmiting positions $\overrightarrow{p_t}(m+n-1)$, $\overrightarrow{p_t}(m+n)$, $\overrightarrow{p_t}(m+n+1)$, and their corresponding times. The estimated $\vec{p}(m)$ is then used to calculate the $\tau_2 = \frac{r_2}{c}$ and the total time delay $\tau = \tau_1 + \tau_2$.

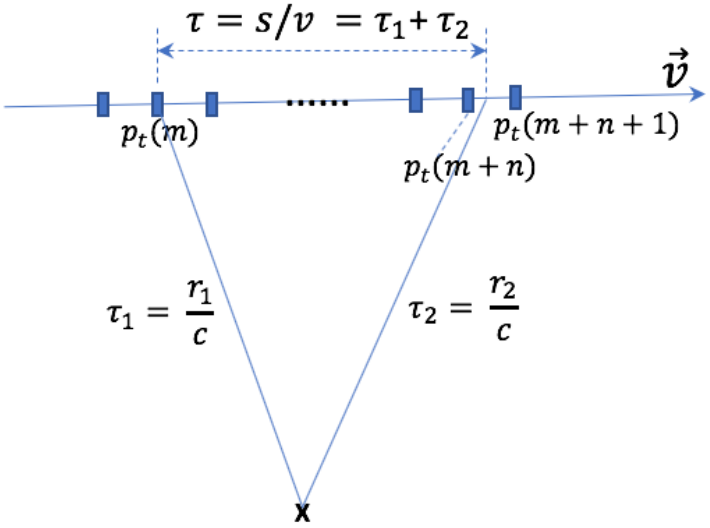

Figure 7 time delay between transmitting pulse and the receiving of the echo.

3.8.5 Accuracy

Other than the numerical errors with the involved calculations including addition/substraction, multiplication/division and square root, the only major error source is the sinc interpolation to calculate the interpolated range compressed data $S\left(\tau\left(\vec{x}, \vec{p}(m), \overrightarrow{p_t}(\vec{x}, m)\right)\right)$. In order to reduce the interpolation error, we oversampled the range compressed data by a factor of 2 using FFT frequency-domain interpolation. The interpolation is done on the oversampled data. In this way the final end-to-end height errors are reduced to the sub-millimeter level. Figure 8 shows 3 point targets from a raw data simulation along with the radar system and platform parameters used for the simulation. Table 2 shows the height errors for the 3 targets at near, middle and far range for both the left and the right sides. The

antenna patterns used for this simulation are gaussian magnitude patterns and zero phase patterns. For each side, the results are divided into two rows. The upper row gives the results for the simulated raw data, where no ADC quantization, 300 MHz to 200 MHz range resampling, presumming, or block floating point quantization (BFPQ) are involved. The lower row gives the resultss for the OBP processed data, where all four of the above operations are assumed. Note that for point targetes, the errors are limited by the effects of the on-board processing (especially BFPQ). Table 3 shows the along track geolocation errors only for left side and the simulated raw data. Fig. 9 shows the mean height error for simulated distributed targets.

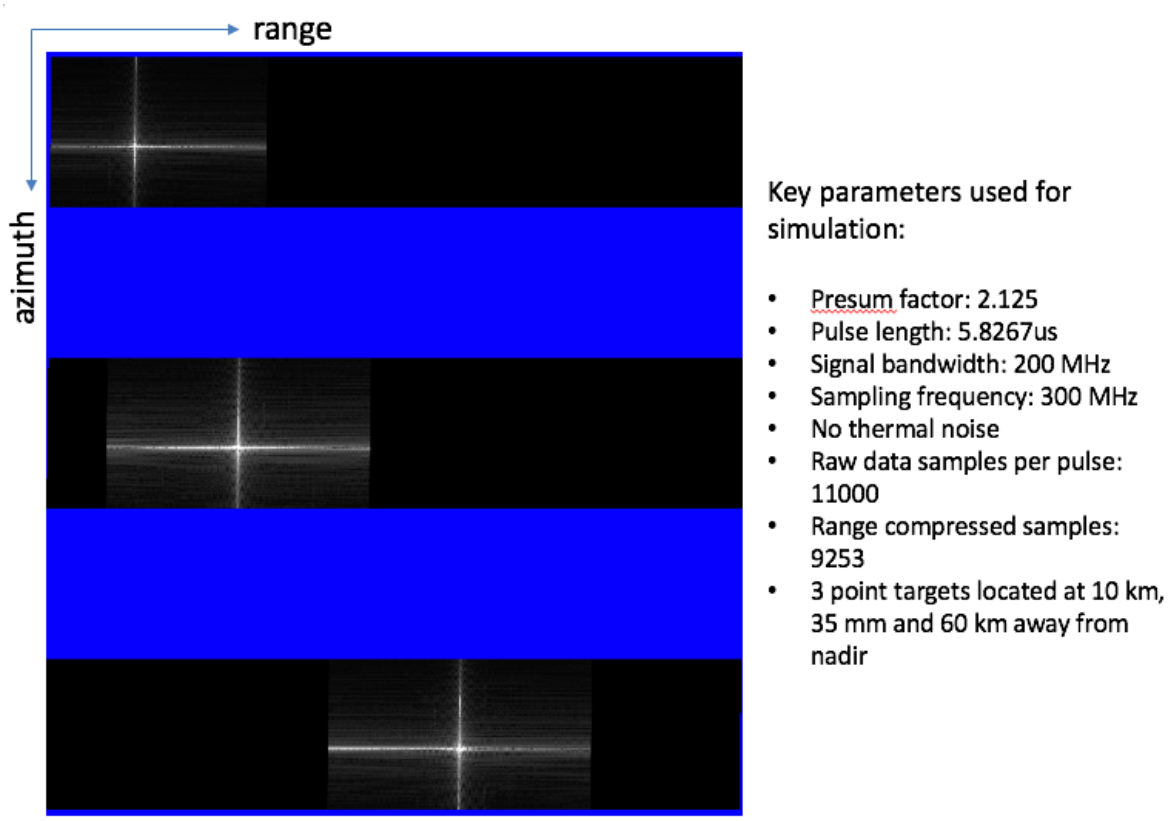

Figure 8 SLC image magnitude of 3 point targets after SLC processor processing of the simulated raw data. The right side shows the key parameters used for raw data simulation.

Table 3 Point target height errors

side		Pts1 (near range)	Pts2 (mid range)	Pts3 (far range)
Left swath	Raw data	*-0.001 mm*	-0.023 mm	-0.129 mm
	After OBP	*-0.043 mm*	-0.205 mm	0.186 mm
Right swath	Raw data	*-0.003 mm*	-0.021 mm	0.136 mm
	After OBP	*-0.015 mm*	0.147 mm	-0.117 mm

Table 4 Point target along track errors

side	Pts1 (near range)	Pts2 (mid range)	Pts3 (far range)
Left swath	*-2.55 mm*	-3.84 mm	-0.32 mm

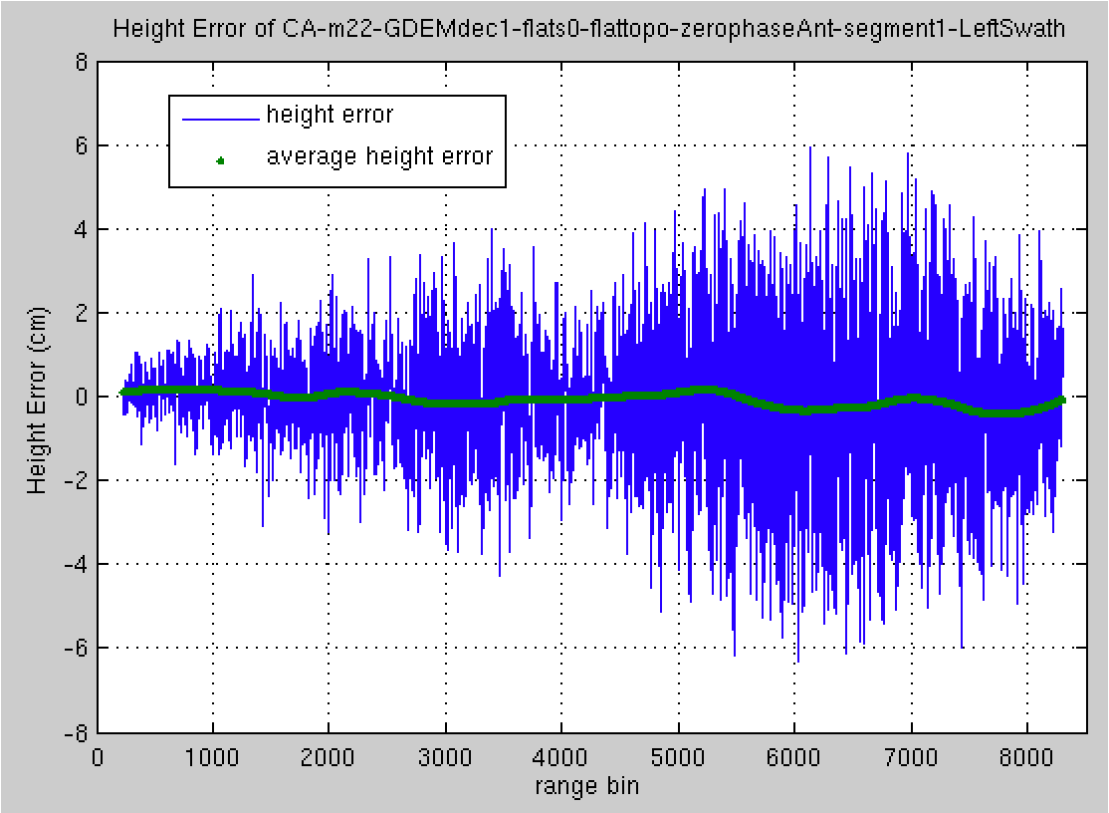

Figure 9 Height error profile from near to far range with range bin size of 0.75m.

3.9 Radiometric Calibration

3.9.1 Purpose

This function computes the radiometric calibration X factor for each image pixel. The X factor will be used in the downstream processing to derive the radar cross section of each image pixel.

3.9.2 Input Data

Description	Source
azimuth compressed data	L1B_SLC_processor
Antenna patterns	Priori antenna pattern files
TVP	ATTD_RECONST, POE / MOE, StaticCal
GrDEM	Reference DEM
Image grid	L1B_SLC_processor

Sensor illumination	L1B_SLC_processor

3.9.3 Output Data

Description
X factor images

3.9.4 Mathematical Statement

The SWOT radiometric calibration algorithm is based on Freeman's paper [7].The raw data power contained in the received echo for each sample can be expressed as:

$$P_{raw} = P_{raw,s} + P_{raw,n} = \frac{P_t G_a^2 \lambda^2 G_r}{(4\pi)^3 R^4} \cdot \frac{c\tau_p}{2sin\theta_i} \cdot \beta_a R \cdot \sigma_0 + P_{raw,n} \quad (27)$$

Where P_{raw} is the total echo power, which includes signal power $P_{raw,s}$, noise power $P_{raw,n}$, P_t is the peak transmit power, G_a is the antenna peak gain, is the wavelength, Gr is the receiver gain, R is the distance between the target and the radar antenna, c is the speed of light, τ_p is the transmit pulse during, θ_i incidence angle, β_a is the antenna 3dB beamwidth, R is the distance between the target and the radar, and σ_0 is the radar cross section per square meters. Note that an effective value of G_a is computed numerically during azimuth compression to account for the actual antenna pattern variation over the synthetic aperture and its dependence on the processed azimuth beamwidth and azimuth resolution. After range and azimuth compression on the raw data, the total power on a SLC image pixel is:

$$P_{slc} = \frac{P_t G_a^2 \lambda^2 G_r}{(4\pi)^3 R^4} \cdot \frac{\rho_r \rho_a}{sin\theta_i} \cdot (n_r n_a)^2 \cdot \sigma_0 + n_r n_a \cdot P_{raw,n} \quad (28)$$

Where ρ_r is range resolution, ρ_a is azimuth resolution, n_r is range compression gain and n_a is azimuth compression gain. Since SWOT HR azimuth compression is using contant processing beamwidth, the azimuth resolution ρ_a is constant. However, the azimuth gain n_a is not a constant and dependent on cross track distance.

In order to calculate the σ_0 more easily, we compensate part of the range and azimuth compression gains by dividing the SLC power with the product $n_r n_a$. After this partial calibration, the SLC power becomes:

$$\bar{P}_{slc} = \frac{P_t G_a^2 \lambda^2 G_r}{(4\pi)^3 R^4} \cdot \frac{\rho_r \rho_a}{sin\theta_i} \cdot n_r n_a \cdot \sigma_0 + P_{raw,n} = X \cdot \sigma_0 + P_{raw,n}, \quad (29)$$

where X is the X factor:

$$X = \frac{P_t G_a^2 \lambda^2 G_r}{(4\pi)^3 R^4} \cdot \frac{\rho_r \rho_a}{sin\theta_i} \cdot n_r n_a. \quad (30)$$

The σ_0 can be simply calculated from

$$\sigma_0 = \frac{\bar{P}_{slc} - P_{raw,n}}{X} \quad . \tag{31}$$

The X factor given in Eq. (30) is output of the function. The $P_{raw,n}$ is estimated by Calibration processor and will be used directly in the downstream pixel cloud processing.

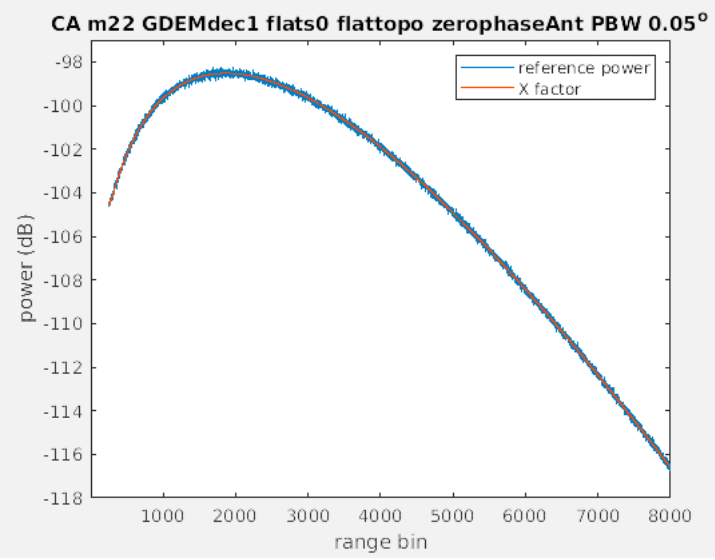

(a) Using processing beamwidth of 0.05°

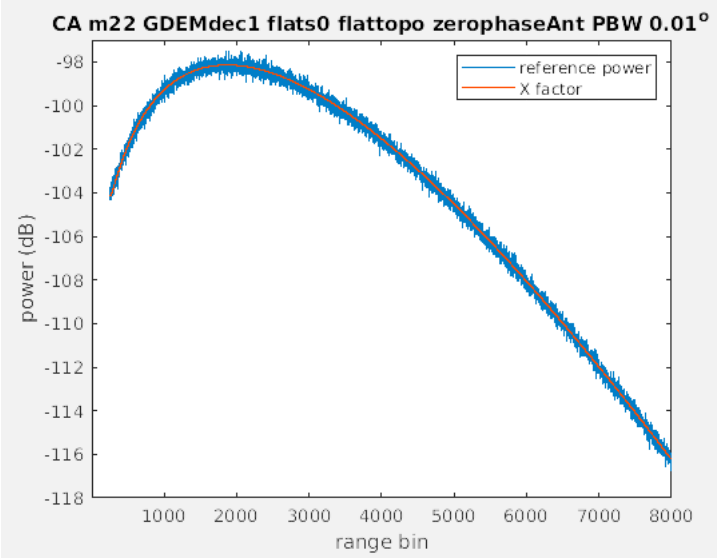

(b) Using processing beamwidth of 0.01°

Fig. 10 *Good match between SLC power and X-factor for different processing beamwidths using simulated raw data. No scaling factor is used.*

Fig. 10 shows the comparison using different processing beamwidths. Fig. 10a is the result of using 0.05 degree processing beamwidth, while Fig. 10b shows the result of using 0.01 degree processing beamwidth. The comparison shows that the calculated Xfactor matches well

with the power of the SLC image of the reference channel.

3.9.5 Accuracy

The accuracy of the calculation of the X factor depends on the accuracy of all the parameters in Eq (30). If they are known perfectly, the mean error of X factor is about zero. Fig. 11 shows the measured SLC power and the predicted SLC power calculated using σ_0 equation from last page. The red line is the X factor and the green curve is the measured SLC power after the noise power is removed. We see a very good match between them. The difference is less than 0.1 dB. SWOT does not have any explicit requirements on radiometric calibration accuracy.

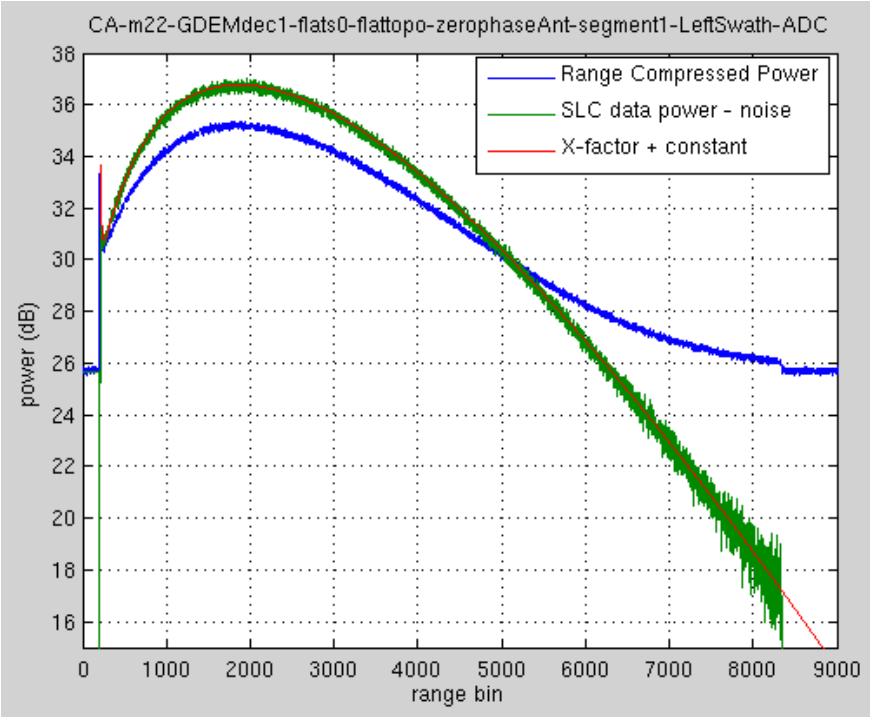

Figure 11 Good match between SLC power and X-factor after noise power is removed

Not all the parameters in Eq. (30) are perfectly known, however. The antenna peak gain G_a is a function the antenna elevation and azimuth angles, which are estimated from the reference DEM. The reference DEM error will cause errors in the antenna elevation angle calculation. A few tens of meters of DEM height error would cause a few dB error in near range in the X factor. The errors in the X factor can be corrected after the correct height reconstruction in the dwon stream processing of pixel cloud processor if desired, but this is not planned.

References

[1] JPL D-61923, "SWOT Science Requirements Document," Jet Propulsion Laboratory Internal Document, 2018.

[2] JPL D-56410, "SWOT Level 1B KaRIn High Rate Single Look Complex Data Product," Jet Propulsion Laboratory Internal Document, 2023.

[3] CLS-GECO-2-09, Version 9.1, "Orbitography functions definitions and specification of the GECO Module," Centre National d'Etudes Spatiales/Collecte Localisation Satellites, 2023.

[4] JPL D-55533, "KaRIn: Ka-band Radar Interferometer On-Board Processor (OBP) for Land Algorithm Theoretical Basis Document," Jet Propulsion Laboratory Internal Document, 2017.

[5] S. Madsen, "Estimating the Doppler Centroid of SAR data," *IEEE Transaction on Aerospace and Electronic Systems,* vol. 25, no. 2, pp. 134-140, 1989, doi:1109/7.18675.

[6] A. Doerry and D. Bickel, "Synthetic Aperture Radar Height of Focus," SAND2021-0144, Sandia Report, Albuquerque, 2021.

[7] A. Freeman and J. Curlander, "Radiometric Correction and Calibration of SAR Images," *Photogrammetric engineering and remote sensing,* vol. 55, no. 9, pp. 1295-1301, 1989.

Appendix A. **Acronyms**

AD	Applicable Document
AMR	Advanced Microwave Radiometer
API	Application Interface
ATBD	Algorithm Theoretical Basis Document
CNES	Centre National d'Études Spatiales
JPL	Jet Propulsion Laboratory
NASA	National Aeronautics and Space Administration
OBP	On-Board Processor
PGE	Product Generation Executable
RD	Reference Document
SAS	Science Algorithm Software
SDS	Science Data System
SWOT	Surface Water Ocean Topography
TAI	Temps Atomique International / International Atomic Time
TBC	To Be Confirmed
TBD	To Be Determined
UTC	Coordinated Universal Time